Chapter 6
Laser-Induced Graphene and Its Applications in Soft (Bio)Sensors

Alexander Dallinger, Kirill Keller, and Francesco Greco

Abstract In recent years the technological importance of graphene increased significantly also in the field of soft, flexible and wearable electronics. In this chapter a simple one step process to create 3D porous graphene structures into flexible polymer films is highlighted. By laser scribing polymer precursor substrates with commercially available laser scribing setups the polymer is converted into so-called Laser-Induced Graphene (LIG) via a photothermal conversion. The properties of this material and the influence of different processing parameters on its composition and structure are introduced. Different transfer methods for stretchable applications are discussed. Three main application fields of LIG for soft (bio)sensors are identified: piezoresistive, electrophysiological and electrochemical sensors. Each of the application fields is highlighted more in detail and an overview of recent publications is given. Concluding with an outlook on the future of LIG – including improvement of patterning resolution and the use of renewable, bio-derived precursors – this chapter provides a broad overview of LIG for soft and flexible sensor devices.

Keywords Laser-induced graphene · Porous carbon · Biosensors · Piezoresistive · Electrophysiological · Electrochemical

A. Dallinger · K. Keller
Institute of Solid State Physics, NAWI Graz, Graz University of Technology, Graz, Austria
e-mail: dallinger@tugraz.at; keller@tugraz.at

F. Greco (✉)
Institute of Solid State Physics, NAWI Graz, Graz University of Technology, Graz, Austria

The Biorobotics Institute, Scuola Superiore Sant'Anna, Pontedera, Italy
e-mail: francesco.greco@santannapisa.it

F. Borghi et al. (eds.), *Nanoporous Carbons for Soft and Flexible Energy Devices*,
Carbon Materials: Chemistry and Physics 11,
https://doi.org/10.1007/978-3-030-81827-2_6

6.1 Introduction

Traditional synthesis of porous carbon involves high temperatures (up to 1200 °C) and an inert atmosphere for thermal decomposition of organic precursors (resins, pitches) [1].

A fairly new method to produce 3D nanoporous graphene, first discovered and investigated by Lin et al., utilizes commercially available CO_2 laser scribing systems to convert insulating polyimide (PI) and other synthetic polymers into conductive Laser-Induced Graphene (LIG), thanks to a photothermal pyrolysis process [2]. This process (schematically depicted in Fig. 6.1) benefits from the absence of any chemicals, no need for inert atmosphere, full and easy customization, and the possibility of converting an insulating polymer substrate into a conductive material while simultaneously patterning it with a desired design. Over the last few years the research interest on LIG has grown steadily, with a focus on the basic understanding of the process, elucidation of its composition and morphology, characterization of its properties, as well as on a myriad of applications, especially in sensing and power storage [3, 4]. Up to date several applications of LIG in devices have been proposed. One of the first devices demonstrated was a microsupercapacitor fabricated from PI [2] followed by stackable [5] and even stretchable supercapacitors [6–8]. Other LIG based devices have been demonstrated, such as: acoustic sensors [9, 10], strain sensors [11–15], gas sensors [16–18], electrophysiological sensors [14, 19, 20] and electrochemical sensors [17, 18, 21–31].

Advancements in applications emerged in parallel with the progresses achieved in the investigation of these materials and of the laser processing required for synthesis. Tuning of composition, surface morphology and properties (i.e. surface, electrical, mechanical) of LIG is achieved by changing the parameters of laser rastering, and mainly the laser fluence H ($J\,cm^{-2}$), defined as the optical energy scribed per surface area [2, 32]. Such control makes it possible to pattern areas of a substrate with specific tailored properties with only one technique. This is

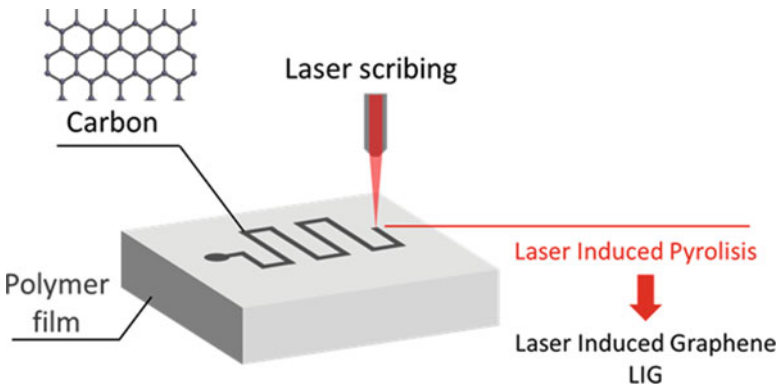

Fig. 6.1 Schematics of laser-induced pyrolysis and LIG creation by laser scribing

especially useful in soft (bio)sensors, where a variety of different requirements have to be fulfilled. Traditional biosensors are electrochemical sensors which can sense biologically relevant substances such as glucose, urea, lactate, among others, with high selectivity, high sensitivity, and low detection limits [33]. Typically, these sensors are developed onto flexible polymer substrates. However, soft biosensors to be deployed in smart skin applications for personal health monitoring do not only need to be flexible but preferably also stretchable and/or conformable. Moreover, in this scenario of skin-worn devices other electrophysiological and piezoresistive sensors are needed, as they can give important information about the health of a person, in addition to the aforementioned biochemical sensing.

A typical sensor consists of a sensing part (transducer) and an electrical interconnection to some wiring or amplification stage. Different sensors have different requirements for the sensing area; for example, in the case of electrochemical sensors often a transducer with high surface area is desired. The transducer is functionalized to achieve the desired sensitivity and selectivity for the target analyte. On the other hand, the electrical connections should have high conductivity. For soft sensors, which can be deformed and bent, the sensing part and the electrical connection should be resistant to changes induced by stress or strain. Even more constraints are given for skin-worn sensors. In addition to the aforementioned resistance to strain the materials should be also biocompatible, adhesive, preferably thin (few μm) and gas (e.g. moisture) permeable. This ensures that the wearable device retains conformability to the epidermis and feels like a second skin for the user.

The following sections of this chapter review the mechanism used to convert polymers into 3D porous graphene and the transfer onto stretchable substrates for the application in soft and epidermal sensors. A detailed survey of the application of LIG in three selected scenarios is then provided: piezoresistive, electrophysiological, electrochemical/gas soft sensors.

6.2 Conversion into 3D Porous Graphene: LIG

Although conversion of PI into amorphous carbon by UV pulsed laser was already known [32], in 2014 Lin et al. accidentally turned some polyimide (PI) into a black conductive porous material by lasering it with a commercial CO_2 laser, routinely used for laser cutting/engraving. This was ascribed to a photothermal pyrolisis process induced by the IR laser scribing in which the polymer precursor, PI, is converted into carbon. The recorded Raman Spectrum of this material unexpectedly showed the characteristic bands associated with graphene instead of typical features of amorphous carbon. A detailed investigation with scanning electron microscopy (SEM), transmission electron microscopy (TEM), X-ray diffraction (XRD), X-ray photoelectron spectroscopy (XPS) and Fourier-Transform infrared spectroscopy (FT-IR) permitted to identify this material as 3D porous graphene which was then named Laser-Induced Graphene (LIG) [2].

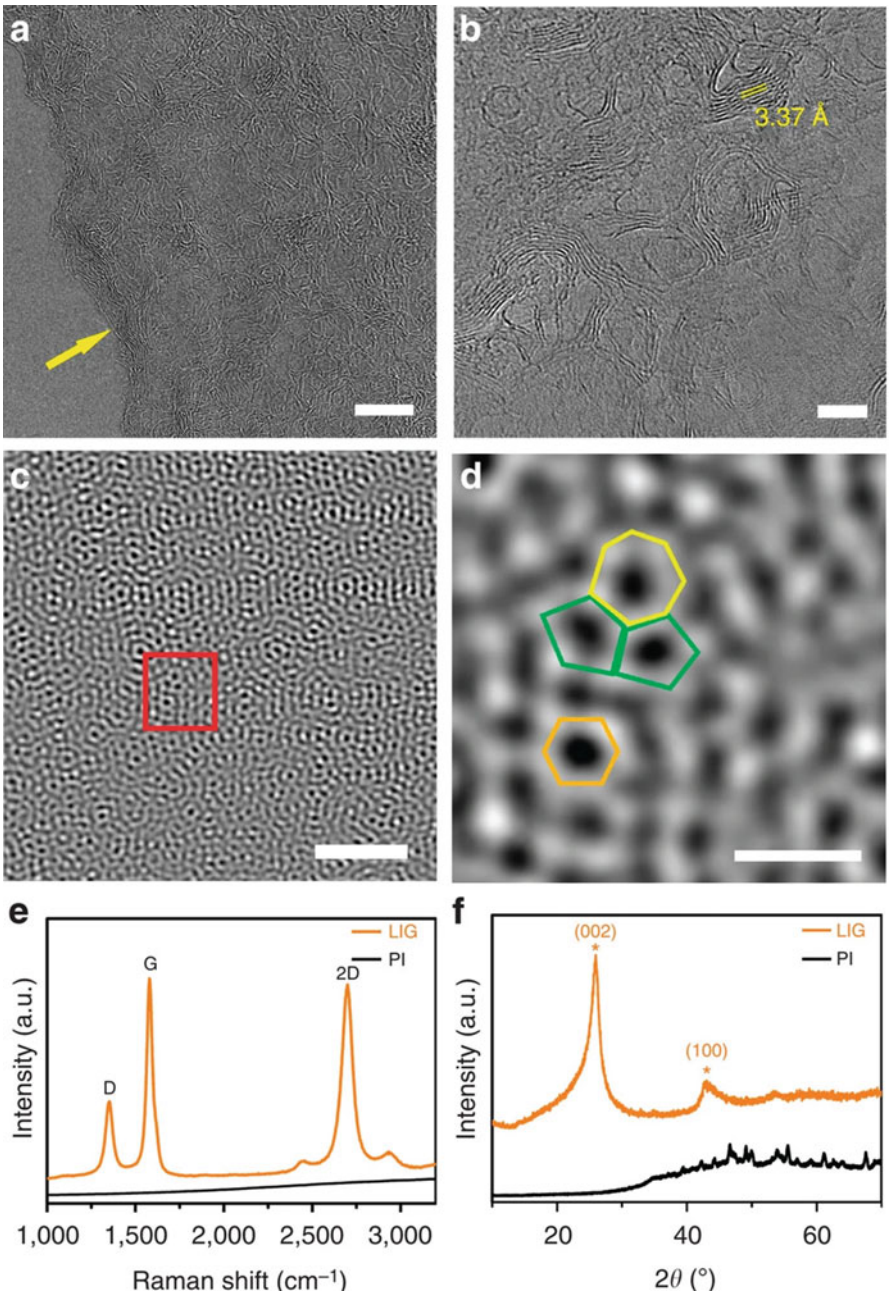

Fig. 6.2 (**a**) TEM image showing wrinkled structures on a cross section of a LIG flake (scale bar: 10 nm); (**b**) detailed view of (**a**) showing a lattice distance of 3.4 Å (scale bar: 5 nm); (**c**, **d**) TEM image showing different types of carbon rings – heptagons, pentagons and hexagons (scale bar: 5 Å); (**e**) Raman Spectrum of LIG scribed into PI; (**f**) XRD for LIG powder from PI. (Reprinted from [2] with permission from Springer Nature)

Further investigations with TEM and XRD showed an average lattice spacing of ≈ 3.4 Å, corresponding to the (002) planes of graphitic materials (Fig. 6.2a, b) [2]. High resolution TEM images revealed that not only the 6-member rings of graphene, but also defective 5- and 7-member rings were present (Fig. 6.2c, d). A typical Raman spectrum for LIG is shown in Fig. 6.2e. In this spectrum one can find three main bands; the first is the D band at ≈1350 cm^{-1}, which is an indicator for defects or bent sp^2 carbon bonds. The second feature, the G band, is located at ≈1580 cm^{-1} while the third feature, the 2D band, is located at ≈2700 cm^{-1}. The 2D band is associated with single layer graphene, the larger width of the band comes from randomly stacked graphene layers. The intensity ratio of D and G bands, I_D/I_G can be used to estimate the degree of crystallinity (graphitization) of the LIG [2].

Investigations with XPS showed that after laser scribing LIG into PI the amount of C-C bonds increased, while the number of C=O, C-O, and C-N bonds decreased (Fig. 6.2f). The data also showed that the carbon is dominated by the sp^2-species, which is in agreement with the Raman and XRD results [2].

Typically the LIG photothermal synthesis is carried out by laser rastering with a CO_2 pulsed laser operating at a 10.6 μm wavelength, commonly used for laser cutting/engraving of various materials. These laser scribing systems comprise focusing optics attaining a typical laser spot size of around 30–100 μm. This size is in fact limiting the resolution of the LIG scribing process. However later studies demonstrated how also UV semiconductor lasers with a wavelength of 405 nm can be used to successfully convert polymers to LIG [25, 34, 35]. With such laser sources smaller beam spot size, and thus improved LIG patterns resolution, is attainable, as recently demonstrated [35].

The photothermal process for creation of LIG depends on the laser energy delivered on the precursor surface during the laser rastering. A characteristic figure used to describe the laser process is thus the laser fluence H, which is calculated as follows, from the laser scribing parameters which can be set in the laser scribing system [14, 32]:

$$H = \frac{P}{s \cdot v \cdot PPI} \tag{6.1}$$

Here the laser fluence H is calculated from the power (P), the laser spot size (s), the scribing speed (v) and the spots per length unit (points per inch, PPI). As the laser fluence is gradually increased, the polymer precursor is increasingly damaged by heat. However the precursor is not turned into LIG until a certain threshold is reached: the critical fluence H_{cr}. For $H < H_{cr}$ no LIG is formed and the material stays an insulator or is simply ablated. Since most of the studies involved PI as a LIG precursor, we will refer to it in the following. For PI, depending on the method of calculation (observed or theoretical spot size) the critical fluence value ranges from $H_{cr} \approx 5\,J\,cm^{-2}$ [32] to $\approx 25\,J\,cm^{-2}$ [14]. For $H > H_{cr}$ LIG is formed and, with increasing fluence, the electrical resistance is correspondingly reduced, up to a point where oxidation starts to play an important role and the resulting gain in reduced resistance gets smaller [2]. For $H > 80\,J\,cm^{-2}$ the PI substrate

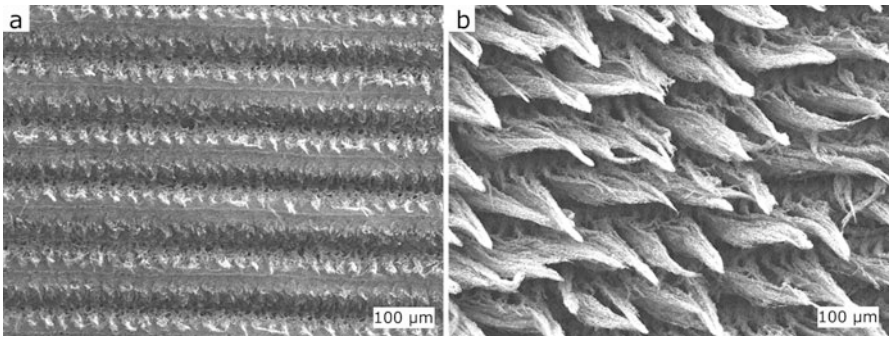

Fig. 6.3 SEM images of flat porous LIG (**a**) (low fluence, H = 25 J cm^{-2}) and fibrous LIG (**b**) (high fluence, H = 50 J cm^{-2}). (Adapted from [14], Copyright © 2020 American Chemical Society, licensed under CC-BY)

gets totally destroyed [14]. Duy et al. investigated how the thickness of scribed LIG was related to the laser fluence H. It was found that with increasing H the thickness of the converted LIG increased [32]. Another parameter affecting much the structure and composition of LIG is the scribing resolution, the combination of PPI (along rastering direction x) and LPI (lines per inch, perpendicular direction to rastering, y) in the so-called raster mode. Duy et al. found that at a scribing resolution of 1000 PPI × 1000 LPI the upper layer of LIG got destroyed because the single laser spots were overlapping. When instead a lower scribing resolution of 500 PPI × 500 LPI was used, fiber-like structures with a length up to 1 mm were emerging from the surface [32]. Dallinger et al. investigated the change of surface morphology by fixing the scribing resolution and changing H. It was found that a threshold $H_{cr} \approx 25\,J\,cm^{-2}$ should be overcome to convert the PI into a flat porous LIG layer (Fig. 6.3a). With $H > 45\,J\,cm^{-2}$ LIG fibers (Fig. 6.3b) started to emerge from the surface; the length of fibers could be varied by changing H. Higher fluence led to longer fibers (up to 1 mm). These individual fibers, with a diameter of around 50 nm to 100 nm, were forming macroscopic bundles of fibers [2, 14] arranged into a so-called "forest".

While a description of the structure and composition of various forms of LIG and how this can be varied by different laser scribing settings has been proposed by several groups, a complete understanding of the LIG formation mechanism is still missing. Molecular dynamics simulations showed that LIG formation happens under high temperature (>2400 K) and pressure (GPa), due to localized laser heating [36]. At these conditions the polymer precursor is decomposed and volatile gases such as CO and H_2 are removed. Depending on the presence of heteroatoms in the pristine macromolecular structure or as additives in the polymer precursor, other compounds can be formed and removed as well. Apart from PI which has a high temperature and chemical resistance and has been the first and more intensively investigated polymer precursor so far, many other polymers were investigated for conversion into LIG. These include Polyetheretherketone (PEEK) [37–39], phenolic

resins [34] and PEI [2]. Poly- or heterocyclic structures seem to be more prone for LIG formation. As the rings break up and the other elements are removed as gases, the sp^3 carbon atoms are converted into sp^2 carbons and create defective graphene structures composed of 5-, 6- and 7-membered carbon rings. The abundance of defective structure could be justified by the kinetics of the process: the system cannot rearrange into an ordered graphitic structure before it is cooled down [40, 41]. Besides many synthetic polymers (for a more complete list the reader is referred to [42]), other biologically derived materials have been successfully converted into LIG. Examples comprise lignin from wood in inert or reducing gas atmosphere [43], wood impregnated with metal salts [44] and lignin from cork, coconut shells and potato skins by multiple lasering [45].

6.3 Properties of LIG

The morphology of LIG has some interesting features arising from the laser scribing process. The laser is rastering over the polymer precursor, while heating and converting it into LIG. The laser beam transversal intensity profile is described by a Gaussian function. Thus, the fluence in the middle of the laser spot is higher than in the outer rim. This results in increased ablation at the center of scribed lines and production of trenches along the laser scribing direction. Also the LIG formed in the middle of the trenches was found to have an higher degree of cristallinity with respect to the one formed at the edges of the trenches, because of such transversal laser fluence gradient [45].

This reflects on the electrical properties of LIG. The electrical resistance measured along the scribing direction is typically lower than the one measured perpendicularly to it [14]. The sheet resistance can be as low as 15 Ω/□ for the flat porous LIG, which gives a conductivity of ≈25 S cm^{-1}, for an estimated homogenous LIG thickness of ≈25 μm [2]. By changing the scribing resolution not only the morphology (from porous to fibers) but also the properties of LIG are changed. By lowering the scribing resolution to obtain fibers, the overlapping of laser pulses and therefore the conductive pathways got less, which resulted in a higher sheet resistance [32].

Another property of LIG which is strongly affected by changing the laser scribing parameters is its surface area. Measurements with the Brunauer–Emmett–Teller (BET) analysis resulted in a surface area for porous LIG of 342 m^2 g^{-1} (pore size <9 nm [2]) and for fibrous LIG of 70 m^2 g^{-1} [32]; in both cases LIG was obtained from PI. The lower surface area of fibrous LIG is due to the fact that the fiber bundles on the surface don't have any pores, while the bulk area has pores formed by the 3D arranged graphene slabs. LIG made from lignin/poly(vinyl acetate) (PVA) films showed a surface area of 338 m^2 g^{-1} and can compete with LIG from PI [46].

Surface wettability of LIG can be changed by tuning the laser parameters. Nasser et al. investigated the change of LIG water wettability depending on the scribing resolution. It was shown that by lowering the resolution from 1000 PPI

to 100 PPI, the wettability of LIG dramatically changed from hydrophilic (full wetting, contact angle (CA) of 0°) to superhydrophobic, with a CA = 161°. XPS and Energy-dispersive X-ray spectroscopy (EDS) investigations showed that by lowering the PPI the oxygen content of produced LIG was decreased. At high resolution scribing the surface was relatively flat and promoted the impregnation of the porous LIG; moreover, the higher oxygen content on the LIG surface promoted its hydrophilic behaviour. Viceversa, at low resolution the emerging LIG fiber pillars create a surface with high roughness at the micro- and nano-scale; additionally, a lower oxygen content is produced. These two combined contributions promote the observed (super)hydrophobic behaviour, according to either a Cassie-Baxter or a Wenzel model [47]. A very interesting finding was that the contact angle was almost negligibly depending on the laser scribing power. However, the sheet resistance could be decreased by 90 % by increasing the laser scribing power [48].

Wu et al. used a two step LIG process for mimicking the taro leaf structure and its peculiar surface properties. The taro leaf's surface structure consists of microscale hexagonal shapes, protruding round shapes and petal-like nanostructures. By recreating this surface pattern by lasering with a Nd:YAG laser at 1064 nm the superhydrophobic behaviour of the taro leaf (CA = 159 ± 2°) could be reproduced (CA = 152°). This was done in a two-steps process: (i) pre-carbonizing the whole PI surface by scribing the PI with a low fluence, and then (ii) laser scribing the pattern onto the surface with a higher fluence [49].

Wettability of LIG depends also on the gas atmosphere used during the laser-induced pyrolysis. Li et al. used a custom chamber equipped with an infrared transparent ZnSe window to scribe PI while flowing different gases (Ar and H_2) through the chamber; the results were then compared with those obtained with scribing in air. The wettability of LIG could be changed from hydrophilic (CA = 0°) in air to superhydrophobic (CA = 157°) in the case of Ar. Investigations with XPS showed that in the case of the (super)hydrophobic samples, made in the reducing (H_2) or inert (Ar) atmosphere, the content of O and C-O in the LIG was lower than in case of scribing in air, and correlated with the higher contact angles [50].

6.4 From Flexible to Stretchable: Transfer onto Substrate

Most polymer precursors which can be converted to LIG are thin enough to be easily bendable and have very good mechanical properties as regards to resistance to repeated mechanical cycling. However they are rather stiff and have a very limited stretchability (up to a few % strain) before showing plastic deformation or even fatal damage/breaking. Thus, flexible sensors can be readily produced by directly scribing LIG circuits and electrodes, but different strategies are required for soft/stretchable (bio)sensors. This is relevant for all those applications where the use of soft and stretchable substrates is required, such as in the case, for example, of epidermal devices. Indeed, applications regarding the placement of sensors on skin require a substrate matching the skin's own mechanical properties.

Moreover, they need to be thin for a conformable application, and have a high water vapor transmission rate (WVTR) in order to let the skin breath and prevent inflammation and discomfort. Currently these requirements can't be fulfilled by any precursor material used for LIG. Therefore, various strategies have been designed and proposed to transfer the conductive LIG pattern onto other soft and stretchable substrates, more suitable for the envisioned applications.

One possible strategy is the embedding of LIG formed on a non stretchable precursor (like PI) into a liquid polymer mixture which can be subsequently crosslinked into a solid elastomeric matrix, like poly-dimethyl siloxane (PDMS) or other thermoset silicones [7, 12, 15, 18, 21, 52]. Here the transfer is achieved by simply submerging the LIG, still anchored to PI, in the elastomer prepolymer mixture, or by blade or spin coating of the latter on top of scribed PI. The liquid can infiltrate into the porous structure of LIG and, after curing, LIG is stably embedded inside the elastomer matrix, forming a composite which can be peeled off from the PI surface (Fig. 6.4a). Luong et al. showed that with this embedding method LIG can be transferred not only onto elastomers but also onto a variety of other materials including solid hydrocarbons, epoxy resins, cement, and geopolymers. This enabled the creation of composite conductive tracks into insulating materials or a local change of wettability of different materials [52].

Some different and very promising strategies have been recently demonstrated. A composite from PDMS and PI particles [53] was prepared. Then an IR laser irradiation caused the conversion in LIG of just the PI phase, and the LIG remained embedded into the soft PDMS matrix. Direct conversion of PDMS into LIG was also demonstrated, but only when operating with a 405 nm UV laser diode [25].

Another method, already known from graphene exfoliation from a block of graphite with a simple scotch tape, is to transfer the LIG from PI with an adhesive surface. By placing the adhesive surface on top of the scribed LIG and applying a pressure, the LIG is transferred from the PI surface to the new one (Fig. 6.4b). This approach was recently used to transfer LIG conductive tracks onto a soft and transparent medical grade polyurethane (PU), enabling various sensing applications on skin [14]. This method can be generalized for allowing the transfer onto almost any solid surface with an adhesive. Here however, differently from the above-mentioned approach of LIG embedded into an elastomer matrix (Fig. 6.4a), the LIG is rather anchored on the elastomer surface and its whole surface can be placed in contact with other target surfaces (as skin) or exposed to analytes (Fig. 6.4b), in case of chemical/biochemical sensors.

Additionally, Li et al. demonstrated a method for industrial scale embedding of LIG into polymer sheets to create several composites. By hot-laminating LIG scribed on PI and thermoplastic sheets (polypropylene, polystyrene, thermoplastic polyurethane and polyvinyl chloride, among others) in a roll-to-roll fashion, different composites were created (Fig. 6.4c) [51].

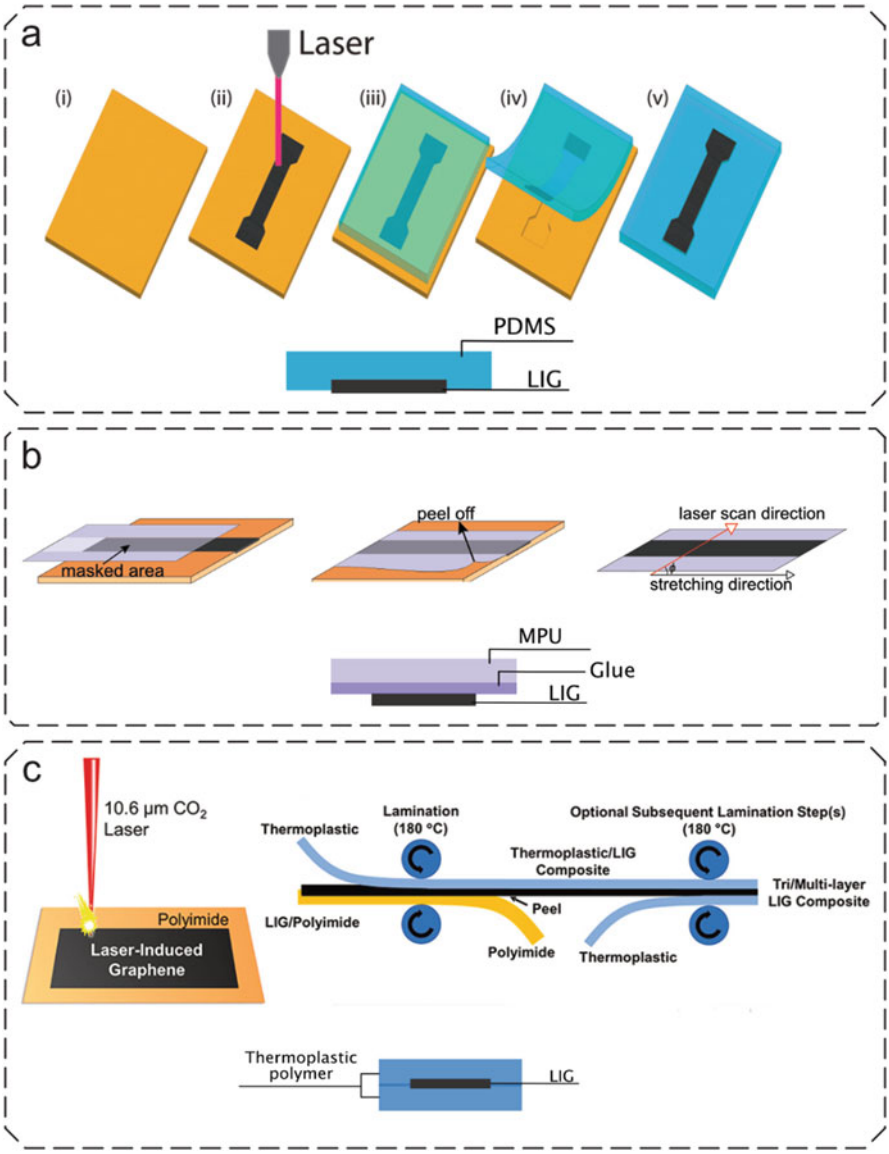

Fig. 6.4 (**a**) Embedding of LIG in PDMS: applying PI tape onto PET sheet (i), scribing of LIG into PI (ii), embedding of LIG it into PDMS (iii), peeling off PDMS with embedded LIG after crosslinking (iv, v). (Adapted with permission from [15] Copyright © 2015 American Chemical Society); (**b**) scribing of LIG into PI and transferring it onto medical polyurethane (MPU). (Adapted from [14] 2020 American Chemical Society, licensed under CC-BY); (**c**) demonstration of roll-to-roll fabrication and lamination for LIG composites. (Adapted from [51], Copyright © 2020 American Chemical Society)

6.5 Applications

The number of studies and proposed applications of LIG has been increasing enormously in the last few years. Some reviews provide a good introduction to the topic and overview of LIG preparation [42], and present its applications in various fields, especially in power storage [54], sensors [3, 4]. Here, given the focus of this chapter, we identified three fields of applications for 3D porous LIG in soft (bio)sensors that will be discussed in more detail: piezoresistive, electrophysiological and electrochemical sensors.

6.5.1 Piezoresistive Sensors

Piezoresistive sensors use the change in resistance observed when the sensor is stretched or compressed. The typical figure that is related to this behaviour is the so-called Gauge Factor (GF),

$$GF = \frac{\Delta R/R}{\Delta L/L} = \frac{\Delta R/R}{\epsilon}. \tag{6.2}$$

The GF sets the change in resistance ($\Delta R/R$ with $\Delta R = R - R_0$) in relation with the change in length, or strain ($\Delta L/L = \epsilon$ with $\Delta L = L - L_0$) of the piezoresistive material structure used as a sensor.

LIG conductors can show a marked piezoresistive behaviour because of crack formation in the conductive matrix during stretching [14, 21]. By changing the laser process parameters (like the fluence H) it is possible to change LIG morphology, which, in turn, results in tuning the GF. Dallinger et al. showed the tuning of GF of LIG-based strain sensors operating under tension and made from medical polyurethane. A porous LIG (LIG-P) produced at low fluence was prone to crack formation and therefore resulted in a higher GF. A fibrous LIG (LIG-F) produced at higher fluence showed a much smaller GF [14]. Another possible strategy for tuning of the GF is to modify the orientation of scribed LIG features with respect to the stretching direction. Scribed LIG lines are more or less prone to crack formation, depending on their orientation. LIG lines scribed parallel to the stretching direction are more prone to irreversible crack formation than those orientated perpendicular to it, as evidenced in some tensile testing experiments [14]. This effect is much dependent on the LPI parameter and thus on the actual separation between consecutively scribed LIG lines. By tuning the LPI parameter the GF can be tuned to some extent.

Another important factor to be considered is the substrate onto which the LIG is transferred and its mechanical properties. While Dallinger et al. used a medical polyurethane, showing a small range of elastic behaviour and an overall pronounced viscoelastic behaviour, Chhetry et al., Wu et al. and Rahimi et al. used PDMS as

a transfer stretchable matrix for LIG. Due to the very good elastic behaviour of PDMS, this resulted in nearly hysteresis-free sensing behaviour [12, 15, 16]. Xuan et al. investigated the influence of the LIG design shape (straight, serpentine) on the GF. A serpentine shape has a significant lower GF than the straight shape, as expected due to geometrical factors impacting on the overall stress applied to the conductor during the application of a tensile strain [21].

The piezoresistive properties of aforementioned LIG composites have found application in biosensing. LIG based piezoresistive epidermal sensors have been demonstrated by wrist pulse detection (Fig. 6.5a) [12, 16], tactile sensing (Fig. 6.5b) [14, 16], measuring the bending angle of a finger (Fig. 6.5c) [12, 15, 16], respiration rate detection [14] and pressure sensing with a sandwich of LIG/PU and polystyrene microspheres [55]. In all these cases, besides the good piezoresistive behaviour, the sensors demonstrated a stable adhesion on skin.

6.5.2 Electrophysiological Sensors

Electrophysiology uses the electrical signals produced by the body, to monitor the body's condition, functioning of organs, muscles, among others. Often this is done with surface (on skin) signal recording, by means of dedicated skin-contact electrodes in so called surface electrophysiology (sEP) recordings [56]. The strongest (larger amplitude) sEP signals come from muscle activation, detected in electromyography (EMG); the heart generates smaller signals measured with electrocardiography (ECG); the smallest and more challenging to detect signals come from brain activity, studied in electroencephalography (EEG). Other electrophysiological techniques exist but we will refer in the following to just these main techniques as they represent the majority of elctrophysiology biosensors presented so far. Commonly Ag/AgCl gel electrodes are used as transducers for sEP, connected to external signal amplification and recording devices. These electrodes use a wet interface to connect to the skin which comes with some major constraints in use, especially for long term recording (manual placement of gel, drying out of gel interface in some hours, interelectrode crosstalk, limited wearing comfort). A possible solution is to use hybrid interfaces (wet/dry) or dry interfaces to connect to the skin. In recent years thin metal films/meshes [57] or tattoo based electrodes based on the conductive polymer poly(3,4-ethylenedioxythiophene):polystyrene sulfonate (PEDOT:PSS) were used [58, 59]. Due to the possibility to embed LIG in flexible and soft/stretchable polymer matrices and to easily pattern them in the desired shape, LIG-based electrodes have been recently tested in this application. Dallinger et al. demonstrated an EMG electrode based on LIG transferred onto medical PU which was worn for 72 h and survived exercising and showering (Fig. 6.6a) with no loss of functionality. The LIG based electrodes could be connected/disconnected multiple times from wiring to external acquisition devices, without suffering from delamination or breaking. The combination of porous LIG and breathable medical polyurethane resulted in an electrode that had high wearing comfort and prevented skin inflammation [14]. Sun et al. embedded LIG into a sugar templated elastomer

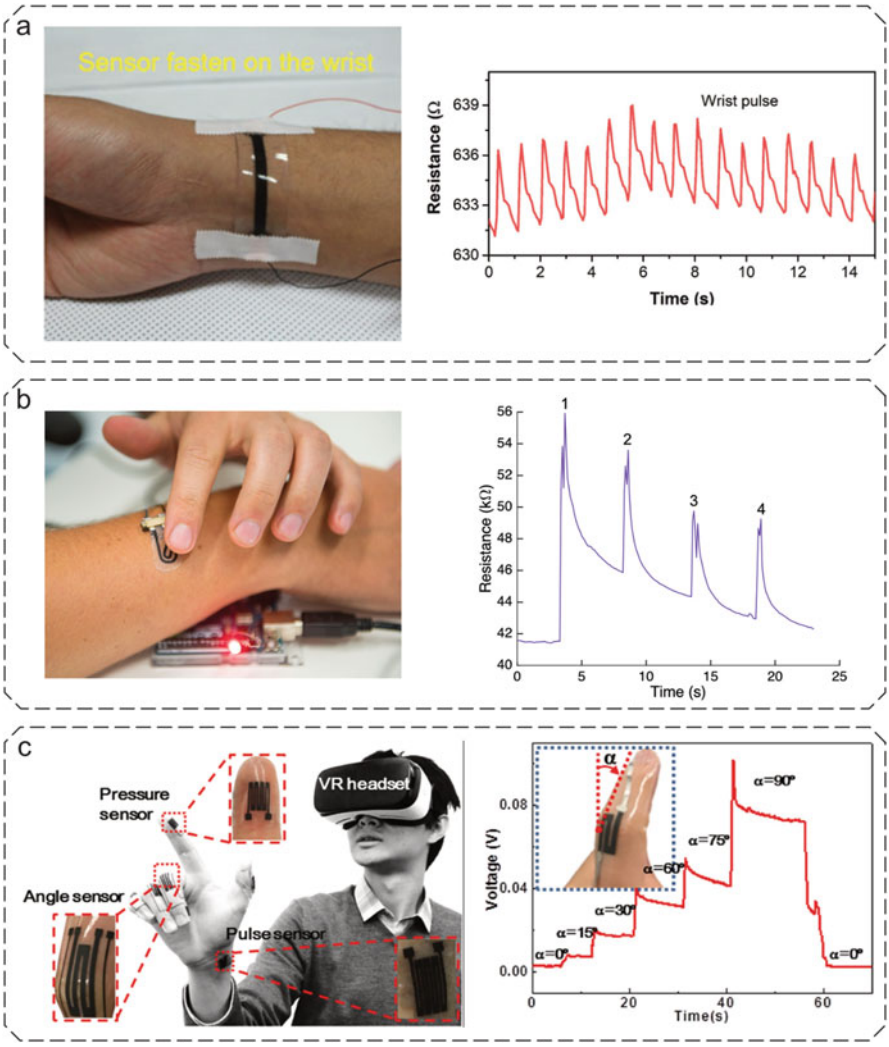

Fig. 6.5 (**a**) Piezoresistive wrist pulse detection by LIG embedded in PDMS. (Adapted from [12], Copyright © 2019 American Chemical Society); (**b**) tactile on-skin button realized with LIG transferred on PI utilizing the piezoresistive effect. (Adapted from [14], Copyright © 2020 American Chemical Society, licensed under CC-BY); (**c**) demonstration of piezoresistive sensor based on LIG/PDMS composite for grip pressure, finger bending angle and pulse sensing. (Reprinted from [16], Copyright © 2018 Elsevier)

sponge with a high water-vapor permeability; these electrodes were used to measure EEG, ECG and EMG in combination with a hydration and temperature sensor (Fig. 6.6b) [19].

Table 6.1 Comparison of the contact impedance at 100 Hz for four different kinds of skin-contact electrodes

Type of electrode	Contact impedance @ 100 Hz	Typology	Reference
Ag/AgCl	12 kΩ	Wet	[19]
	80 kΩ	Wet	[58]
Au Nanomesh	140 kΩ	Dry	[19]
LIG	17 kΩ	Dry	[19]
PEDOT:PSS	100 to 200 kΩ	Dry	[58]

An ECG sensor demonstrated by Zahed et al. used LIG scribed onto PI and spray coating of PEDOT:PSS to sense the heartbeat when placing a thumb of one hand, and the index and middle fingers of another hand on the sensor and pressing against it (Fig. 6.6c). Thus, this approach is very different from those reviewed so far, since it doesn't imply embedding of LIG electrodes into a wearable. The spray coating of LIG with PEDOT:PSS significantly enhanced the adhesion to PI and the mechanical resistance against rubbing [20].

Comparing the contact impedance of different types of electrodes at 100 Hz (as relevant in several electrophysiology techniques) shows that LIG electrodes are performing as good as other types (Table 6.1).

6.5.3 Electrochemical Sensors

Analysis of many biofluids, biomolecules and even cells and bacteria can rely on powerful electrochemical analysis methods. Electrochemical sensors could be single or multielectrode systems. The most dominant are three electrode sensors which include working electrode (WE), counter electrode (CE) and reference electrode (RE) [60]. In most cases CE is just a conductor several times larger than WE to reduce the resistance at solution/WE interface. RE consists of the material with known electrochemical potential and is used to compare the potential of the WE. In wearable applications RE is commonly made of Ag/AgCl. Ag/AgCl electrodes are easy to fabricate with multiple methods; they are based on solid state chemical equilibrium and suitable for use in water-based environments such as body fluids (e.g. sweat) as relevant for many health monitoring, ex vivo as well as in vivo, both inside the body (implanted sensors) or surface (sensors mounted on skin).

In an electrochemical sensor the WE is responsible for selective sensing of the analyte. The WE is usually made of conductive material functionalized with some solvent resistant species. The huge surface area of LIG in combination with its good intrinsic conductivity allows to easily modify it, adding an extremely wide range of selective functionality. So far there are many reports of adapting LIG for electrochemical sensors. The simplest example of an electrochemical LIG-sensor can include only a single electrode. Zhang et al. presented an electrochemical

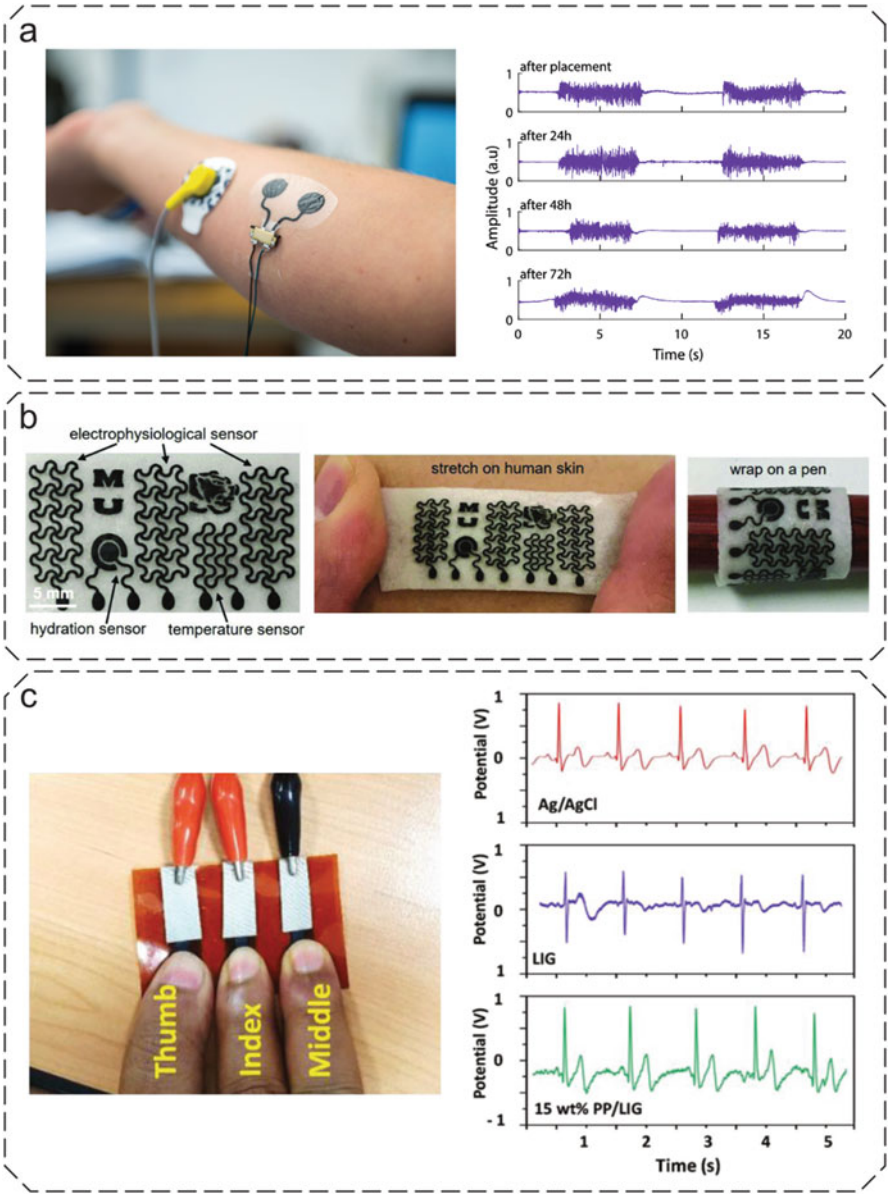

Fig. 6.6 (**a**) Electromyography (EMG) sensor based on LIG transferred onto medical polyurethane. (Adapted from [14], Copyright © 2020 American Chemical Society, licensed under CC-BY); (**b**) electrophysiological sensor based on sugar-templated elastomer sponge with embedded LIG. (Adapted from [19], Copyright © 2018 WILEY-VCH Verlag GmbH & Co. KGaA, Weinheim); (**c**) LIG/PEDOT:PSS composite for electrocardiography (ECG) recording on finger tips. (Reprinted from [20], Copyright © 2020 Elsevier)

sensor for detection of trans-resveratrol (TRA), a natural polyphenol isomer found in many plants, including grapes. The sensor was used to quantitatively determine the content of TRA in red wines. It was composed of a pure LIG electrode lasered from PI sheet [30]. The sensor wasn't functionalized at all, but before use it needed activation with several cycles of cyclic voltammetry (CV) sweeping in PBS solution to remove organic impurities from inside the porous structure. Even such simple configuration could be used to determine TRA concentration with differential pulse voltammetry (DPV). A similar concept was used in [31], where laser parameters were tuned to incorporate more nitrogen atoms into graphene composition and form N-doped LIG with improved sensitivity; the sensor was used to analyse micro-RNA molecules with limit of detection (LOD) of 10 fmol. Recently LIG electrodes formed on PI were functionalized with antibodies (Fig. 6.7a) for detection of *S. enterica* bacteria [27]. This sensor showed high selectivity for target bacteria even in complex media and broad range of detection from 25 CFU/mL to 10×10^5 CFU/mL (colony-forming unit). Bacteria concentration was measured using electrochemical impedance spectroscopy.

Multielectrode sensors on LIG include skin pH sensors where the function of WE and CE are combined into a single electrode [21, 22]. The WE is electrochemically functionalized mainly with polyaniline (PANI) aqueous solution because it is non-toxic, skin-friendly and has high pH-sensitivity. Demonstrated sensors exhibit high pH-response (66 in [21] and 75 in [22] mV/pH) in the range 4 pH to 7 pH.

Using complex electrochemical analysis techniques such as CV requires implementing full three electrodes design. More sophisticated sensors could be functionalized with enzymes which exchange the electrons with the target molecule under applied potential. For example for glucose sensors glucose oxidase (GOx) is widely used [62], and most of the work aimed on improving electromechanical properties of fabricated devices. One of the first examples of GOx-based sensors on LIG was shown by Zhang et al. [34]. All three electrodes were lasered from the spin-coated phenolic resin film "doped" with $FeCl_3$. Afterwards the GOx with ferrocene acting as an electron-transfer mediator, were encapsulated onto WE in a chitosan hydrogel. Presented biosensor showed good sensitivity to glucose (LOD 0.2 mmol), however selectivity was not tested. One way to improve the sensor's limit of detection is to reduce the resistivity of the LIG. Currently, most common way is to use the combination of metal nanoparticles electroplating (Fig. 6.7b) inside the LIG pores and some solution-based additive for the interface modification, including: PEDOT:PSS spraying [22], and treatment with acetic acid to increase the content of C-C bonds [23]. Lately, the first attempts to solve the wearability issue of such electrochemical glucose sensors were demonstrated by Xuan et al. by coupling of LIG with PDMS by silver nanowires (AgNW) [21]. AgNW provided better piezoresistive properties up to 40 % strain with the R/R_0 ratio reaching thousands percent. The electrochemical properties were also enhanced by electroplating of Au/Pt nanoparticles inside LIG pores which improved electron-transfer rate. Apart from glucose biosensors, three electrode design are also suitable for detection of other organic molecules, e.g. chloramphenicol – an important antibiotic contaminant

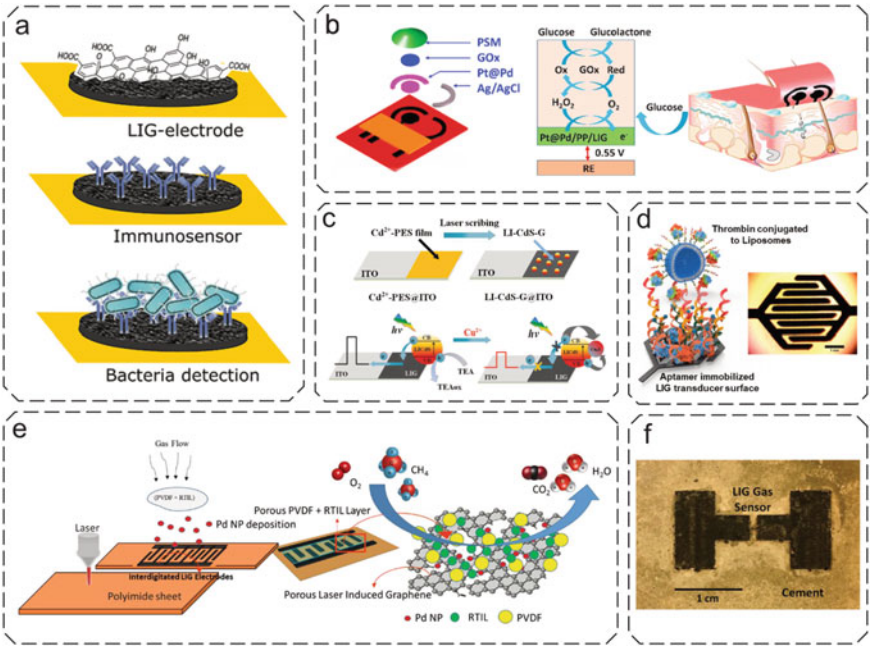

Fig. 6.7 LIG-based bio-, electrochemical and gas sensors; (**a**) LIG imunosensor functionalized with antibodies for bacteria detection. (Adapted with permission from [27] Copyright © 2020, American Chemical Society); (**b**) illustration of LIG-based glucose biosensor assembly and working principle. (Reprinted with permission from [22], Copyright © 2020 Elsevier); (**c**) LIG photoelectrode fabrication and working principle. (Adapted from [61] with permission from © 2019 WILEY-VCH Verlag GmbH & Co. KGaA, Weinheim); (**d**) LIG IDEs for thrombin detection. (Reprinted permission from [29], Copyright © 2020 Elsevier); (**e**) electrochemical methane LIG-sensor. (Reprinted with permission from [26], Copyright © 2019, American Chemical Society); (**f**) LIG gas sensor embedded into cement. (Adapted with permission from [17], Copyright © 2019 American Chemical Society)

in agriculture [28]. WE in the presented device was modified with a molecularly imprinted polymer and had a LOD 0.62 nmol.

Non-enzymatic LIG-based sensors have started to emerge recently. A method was developed to produce the decorated LIG from the mixture of liquid polymer precursors and metal complexes. First example of the photoelectrode made of LIG was formed from a mixture of Ti^{4+} and poly(amic acid) (PAA) solution [63]. Furthermore, this concept was employed for fabrication of metal sulfide doped LIG from polyethersulfone precursor as a photoelectrode, which could also be adapted for selective photoelectrochemical sensing of Cu^{2+} (Fig. 6.7c) [61]. One of the most promising is the photoelectrode-based glucose sensor made by direct lasering of PES membrane mixed with Cd/Ni complexes [24]. Resulting LIG was already doped with metal ions which act as photocatalytic sites for glucose oxidation.This

sensor is simpler in production since it doesn't need additional electrodes and demonstrates a LOD in the order of micromoles.

Special cases of sensors with electrochemical nature are interdigitated electrodes (IDEs) made of LIG. These sensors (Fig. 6.7d) could be used for capacitive detection of thrombin, upon surface functionalization of LIG [29]. Dosi et al. studied application of LIG IDEs decorated with Pd nanoparticles for alkane sensing (Fig. 6.7e) [26]. Pd-doped LIG covered with solid polymer electrolyte promotes electrooxidation of methane gas. The LOD of the sensor is quite low and is around 9 ppm, however the sensor is also sensitive to interfering low-molecular weight alkanes which affects the accuracy in complex gaseous mixtures. LIG decorated with nanostructured ZnO is interesting because of its active UV sensing capabilities [64]. In this case LIG electrodes are treated with UV/ozone to improve wetting and allow drop-casted ZnO dispersion to evenly distribute inside the pores of the carbon structure. Sensor performance was tested by measuring the photocurrent under UV light and it was found that the sensitivity is highly dependent on the geometry of IDEs.

6.5.4 Gas Sensors

A special class of LIG-based sensing devices are flexible and embeddable gas sensors. The already demonstrated decoration of LIG with nanoparticles, in combination with other physical concepts might help in creation of so called "artificial nose" in future.

LIG decorated with Pd NPs was demonstrated to be an accurate hydrogen sensor with sensitivity at room temperature down to 600 ppm [25]. The sensing mechanism is based on the well known catalytic effect of Pd and on its structural changes upon adsorption of H_2. Another approach relies on decoration of LIG with reduced graphene (rGO)/MoS_2 particles [18]. The formed composite electrode acts as a chemiresistor which exhibits an ultrasensitive detection of NO_2 gas with LOD of 1.5 ppb.

One of the most accurate and selective sensors so far are sensors based on thermal conductivity of gases, known as thermal conductivity detectors or katharometers. Very thin channel (50–60 μm) is lasered between 2 electrodes and when potential is applied the channel starts heating [17]. This causes the change in resistance which depends on the thermal conductivity of surrounding gas. With these sensors it is possible to detect CO_2, O_2, N_2 from a binary gas mixture (He, Ar) with sensitivity down to 1000–3000 ppm and response time around 8 s. Due to the ability to transfer the LIG onto different surfaces, the katharometer LIG-based sensor was transferred onto cement (Fig. 6.7f) allowing to deploy it in extreme conditions.

6.6 Outlook

In the previous sections we have shown how in recent years the conversion of polymers into LIG by direct laser writing gained a lot of interest for both fundamental and applied research. Here we aim to highlight some current and future challenges that could permit to develop even further the LIG preparation and its use in devices. Improvements in LIG processing can still be achieved by lowering the minimum feature size of LIG by using a UV laser [35]. Lasering with CO_2 lasers actually causes direct heating and "burn" of the polymer, which results in a LIG feature larger than the actual laser spot size. Compared to this, UV lasers locally heat the substrate by absorption and thus a smaller LIG features can be obtained. In order to minimize the price and environmental footprint of LIG-based materials, it will be important to find alternative precursors (preferably bioderived) for LIG conversion. An already demonstrated possible route is the use of an inert atmosphere (e.g. N_2) during laser scribing of biologically derived materials [43]. A very promising approach is the use of lignin as a precursors for LIG, either as a composite consisting of poly(ethylene oxide) (PEO) [65, 66] or poly(vinyl acetate) (PVA) [46, 67] and lignin. Edberg et al. demonstrated an ink based on lignin and cellulose (2-HEC) which was used for screen printing patterns on top of surfaces which were afterwards converted to LIG via scribing with a CO_2 laser [68].

Another way to scale up LIG preparation into industrial scale production is represented by a roll-to-roll (R2R) production. Li et al. showed that it is possible to create composites with LIG by just using a commercially available thermal laminator. Sheets of polypropylene, polystyrene, polyurethane and other thermoplastic materials were laminated to composites with LIG [51]. By further improving the aforementioned approaches, LIG can become a cheap, scalable and reliable technology for sensor fabrication. The laser scribing process allows for an easy and local tuning of properties which enables the creation of a multifunctional device in one go (e.g. electrophysiological, temperature and hydration [19]). The highly porous nature of LIG makes it the perfect base for electrochemical sensors, due to the high surface area which can be utilized for surface functionalization. By using different functionalization chemicals and methods, multifunctional electrochemical sensors can be achieved (e.g. pH and glucose [21, 22]). LIG shows as well a great potential to act as an electrode for supercapacitors, especially in flexible [69–71] and stretchable/wearable supercapacitors [5–7] . Further improving the supercapacitors performance, in combination with wireless communication and powering (such as NFC or RFID) can enable wearable devices to be self powered. As regards future directions in bioapplications, first toxicity assessments on LIG have been carried out on zebrafish [72], suggesting that LIG could be safely used in biological/biomedical applications. Additionally, by finding alternative (e.g. biodegradable, edible) precursors, LIG could be used in the development of next generation transient [73] and even edible electronics [45, 74].

References

1. Inagaki, M.: New Carbons Control of Structure and Functions. Elsevier Science, Amsterdam/New York (2000)
2. Lin, J., Peng, Z., Liu, Y., Ruiz-Zepeda, F., Ye, R., Samuel, E.L.G., Yacaman, M.J., Yakobson, B.I., Tour, J.M.: Laser-induced porous graphene films from commercial polymers. Nat. Commun. **5**, 5714 (2014)
3. Huang, L., Su, J., Song, Y., Ye, R.: Laser-induced graphene: En route to smart sensing. Nano-Micro Lett. **12**, 157 (2020)
4. Wan, Z., Nguyen, N.-T., Gao, Y., Li, Q.: Laser induced graphene for biosensors. Sustainable Mater. Technol. **25**, e00205 (2020)
5. Peng, Z., Lin, J., Ye, R., Samuel, E.L.G., Tour, J.M.: Flexible and stackable laser-induced graphene supercapacitors. ACS Appl. Mater. Interfaces **7**, 3414–3419 (2015)
6. Lamberti, A., Clerici, F., Fontana, M., Scaltrito, L.: A highly stretchable supercapacitor using laser-induced graphene electrodes onto elastomeric substrate. Adv. Energy Mater. **6**, 1600050 (2016)
7. Song, W., Zhu, J., Gan, B., Zhao, S., Wang, H., Li, C., Wang, J.: Flexible, stretchable, and transparent planar microsupercapacitors based on 3D porous laser-induced graphene. Small **14**, 1702249 (2018)
8. Tehrani, F., Beltrán-Gastélum, M., Sheth, K., Karajic, A., Yin, L., Kumar, R., Soto, F., Kim, J., Wang, J., Barton, S., Mueller, M., Wang, J.: Laser-induced graphene composites for printed, stretchable, and wearable electronics. Adv. Mater. Technologies **4**, 1900162 (2019)
9. Tao, L.-Q., Tian, H., Liu, Y., Ju, Z.-Y., Pang, Y., Chen, Y.-Q., Wang, D.-Y., Tian, X.-G., Yan, J.-C., Deng, N.-Q., Yang, Y., Ren, T.-L.: An intelligent artificial throat with sound-sensing ability based on laser induced graphene. Nat. Commun. **8**, 14579 (2017)
10. Zhang, P., Tang, X., Pang, Y., Bi, M., Li, X., Yu, J., Zhang, J., Yuan, M., Luo, F.: Flexible laser-induced-graphene omnidirectional sound device. Chem. Phys. Lett. **745**, 137275 (2020)
11. Carvalho, A.F., Fernandes, A.J.S., Leitão, C., Deuermeier, J., Marques, A.C., Martins, R., Fortunato, E., Costa, F.M.: Laser-induced graphene strain sensors produced by ultraviolet irradiation of polyimide. Adv. Funct. Mater. **28**, 1805271 (2018)
12. Chhetry, A., Sharifuzzaman, M., Yoon, H., Sharma, S., Xuan, X., Park, J.Y.: MoS2-decorated laser-induced graphene for a highly sensitive, hysteresis-free, and reliable piezoresistive strain sensor. ACS Appl. Mater. Interfaces **11**, 22531–22542 (2019)
13. Liu, W., Huang, Y., Peng, Y., Walczak, M., Wang, D., Chen, Q., Liu, Z., Li, L.: Stable wearable strain sensors on textiles by direct laser writing of graphene. ACS Appl. Nano Mater. **3**, 283–293 (2020)
14. Dallinger, A., Keller, K., Fitzek, H., Greco, F.: Stretchable and skin-conformable conductors based on polyurethane/laser-induced graphene. ACS Appl. Mater. Interfaces **12**, 19855–19865 (2020)
15. Rahimi, R., Ochoa, M., Yu, W., Ziaie, B.: Highly stretchable and sensitive unidirectional strain sensor via laser carbonization. ACS Appl. Mater. Interfaces **7**, 4463–4470 (2015)
16. Wu, Y., Karakurt, I., Beker, L., Kubota, Y., Xu, R., Ho, K.Y., Zhao, S., Zhong, J., Zhang, M., Wang, X., Lin, L.: Piezoresistive stretchable strain sensors with human machine interface demonstrations. Sens. Actuators A **279**, 46–52 (2018)
17. Stanford, M.G., Yang, K., Chyan, Y., Kittrell, C., Tour, J.M.: Laser-induced graphene for flexible and embeddable gas sensors. ACS Nano **13**, 3474–3482 (2019)
18. Yang, L., Yi, N., Zhu, J., Cheng, Z., Yin, X., Zhang, X., Zhu, H., Cheng, H.: Novel gas sensing platform based on a tretchable laser-induced graphene pattern with self-heating capabilities. J. Mater. Chem. A **8**, 6487–6500 (2020)
19. Sun, B., McCay, R.N., Goswami, S., Xu, Y., Zhang, C., Ling, Y., Lin, J., Yan, Z.: Gas-permeable, multifunctional on-skin electronics based on laser-induced porous graphene and sugar-templated elastomer sponges. Adv. Mater. **30**, 1804327 (2018)

20. Zahed, M.A., Das, P.S., Maharjan, P., Barman, S.C., Sharifuzzaman, M., Yoon, S.H., Park, J.Y.: Flexible and robust dry electrodes based on electroconductive polymer spray-coated 3D porous graphene for long-term electrocardiogram signal monitoring system. Carbon **165**, 26–36 (2020)
21. Xuan, X., Kim, J.Y., Hui, X., Das, P.S., Yoon, H.S., Park, J.-Y.: A highly stretchable and conductive 3D porous graphene metal nanocomposite based electrochemical-physiological hybrid biosensor. Biosens. Bioelectron. **120**, 160–167 (2018)
22. Zahed, M.A., Chandra Barman, S., Das, P.S., Sharifuzzaman, M., Yoon, H.S., Yoon, S.H., Park, J.Y.: Highly flexible and conductive poly (3, 4-ethylene dioxythiophene)-poly (styrene sulfonate) anchored 3-dimensional porous graphene network-based electrochemical biosensor for glucose and pH detection in human perspiration. Biosens. Bioelectron. **160**, 112220 (2020)
23. Yoon, H., Nah, J., Kim, H., Ko, S., Sharifuzzaman, M., Barman, S.C., Xuan, X., Kim, J., Park, J.Y.: A chemically modified laser-induced porous graphene based flexible and ultrasensitive electrochemical biosensor for sweat glucose detection. Sens. Actuators B **311**, 127866 (2020)
24. Li, H., Guo, C., Liu, C., Ge, L., Li, F.: Laser-induced graphene hybrid photoelectrode for enhanced photoelectrochemical detection of glucose. Analyst **145**, 4041–4049 (2020)
25. Zhu, J., Cho, M., Li, Y., Cho, I., Suh, J.-H., Orbe, D.D., Jeong, Y., Ren, T.-L., Park, I.: Biomimetic turbinate-like artificial nose for hydrogen detection based on 3D porous laser-induced graphene. ACS Appl. Mater. Interfaces **11**, 24386–24394 (2019)
26. Dosi, M., Lau, I., Zhuang, Y., Simakov, D.S.A., Fowler, M.W., Pope, M.A.: Ultrasensitive electrochemical methane sensors based on solid polymer electrolyte-infused laser-induced graphene. ACS Appl. Mater. Interfaces **11**, 6166–6173 (2019)
27. Soares, R.R.A., Hjort, R.G., Pola, C.C., Parate, K., Reis, E.L., Soares, N.F.F., McLamore, E.S., Claussen, J.C., Gomes, C.L.: Laser-induced graphene electrochemical immunosensors for rapid and label-free monitoring of Salmonella Enterica in chicken broth. ACS Sensors **5**, 1900–1911 (2020)
28. Cardoso, A.R., Marques, A.C., Santos, L., Carvalho, A.F., Costa, F.M., Martins, R., Sales, M.G.F., Fortunato, E.: Molecularly-imprinted chloramphenicol sensor with laser-induced graphene electrodes. Biosens. Bioelectron. **124–125**, 167–175 (2019)
29. Yagati, A.K., Behrent, A., Beck, S., Rink, S., Goepferich, A.M., Min, J.,Lee, M.-H., Baeumner, A.J.: Laser-induced graphene interdigitated electrodes for label-free or nanolabel-enhanced highly sensitive capacitive Aptamer-based biosensors. Biosens. Bioelectron. **164**, 112272 (2020)
30. Zhang, C., Ping, J., Ying, Y.: Evaluation of trans-resveratrol level in grape wine using laser-induced porous graphene-based electrochemical sensor. Sci. Total Environ. **714**, 136687 (2020)
31. Wan, Z., Umer, M., Lobino, M., Thiel, D., Nguyen, N.-T., Trinchi, A., Shiddiky, M.J., Gao, Y., Li, Q.: Laser induced self-N-doped porous graphene as an electrochemical biosensor for femtomolar miRNA detection. Carbon **163**, 385–394 (2020)
32. Duy, L.X., Peng, Z., Li, Y., Zhang, J., Ji, Y., Tour, J.M.: Laser-induced graphene fibers. Carbon **126**, 472–479 (2018)
33. Zhai, Q., Cheng, W.: Soft and stretchable electrochemical biosensors. Mater. Today Nano **7**, 100041 (2019)
34. Zhang, Z., Song, M., Hao, J., Wu, K., Li, C., Hu, C.: Visible light laser-induced graphene from phenolic resin: a new approach for directly writing graphene-based electrochemical devices on various substrates. Carbon **127**, 287–296 (2018)
35. Stanford, M.G., Zhang, C., Fowlkes, J.D., Hoffman, A., Ivanov, I.N., Rack, P.D., Tour, J.M.: High-resolution laser-induced graphene. Flexible electronics beyond the visible limit. ACS Appl. Mater. Interfaces **12**, 10902–10907 (2020)
36. Dong, Y., Rismiller, S.C., Lin, J.: Molecular dynamic simulation of layered graphene clusters formation from polyimides under extreme conditions. Carbon **104**, 47–55 (2016)
37. Lamberti, A., Serrapede, M., Ferraro, G., Fontana, M., Perrucci, F., Bianco, S., Chiolerio, A., Bocchini, S.: All-SPEEK flexible supercapacitor exploiting laser-induced graphenization. 2D Mater. **4**, 035012 (2017)

38. Zhu, C., Zhao, D., Wang, K., Dong, X., Duan, W., Wang, F., Gao, M., Zhang, G.: Direct laser writing of graphene films from a polyether ether ketone precursor. J. Mater. Sci. **54**, 4192–4201 (2019)
39. Yang, W., Zhao, W., Li, Q., Li, H., Wang, Y., Li, Y., Wang, G., Fabrication of smart components by 3D printing and laser-scribing technologies. ACS Appl. Mater. Interfaces **12**, 3928–3935 (2020)
40. Vashisth, A., Kowalik, M., Gerringer, J., Ashraf, C., van Duin, A.C., Green, M.J.: ReaxFF simulations of laser-induced graphene (LIG) formation for multifunctional polymer nanocomposites, ACS Appl. Nano Mater. **3**, 1881–1890 (2020)
41. Chen, Y., Long, J., Zhou, S., Shi, D., Huang, Y., Chen, X., Gao, J., Zhao, N., Wong, C.-P.: UV laser-induced polyimide-to-graphene conversion: modeling, fabrication, and application. Small Methods **3**, 1900208 (2019)
42. Wang, F., Wang, K., Zheng, B., Dong, X., Mei, X., Lv, J., Duan, W., Wang, W.: Laser-induced graphene: preparation, functionalization and applications. Mater. Technol. **33**, 340–356 (2018)
43. Ye, R., Chyan, Y., Zhang, J., Li, Y., Han, X., Kittrell, C., Tour, J.M.: Laser-induced graphene formation on wood. Adv. Mater. **29**, 1702211 (2017)
44. Han, X., Ye, R., Chyan, Y., Wang, T., Zhang, C., Shi, L., Zhang, T., Zhao, Y., Tour, J.M.: Laser-induced graphene from wood impregnated with metal salts and use in electrocatalysis. ACS Appl. Nano Mater. **1**, 5053–5061 (2018)
45. Chyan, Y., Ye, R., Li, Y., Singh, S.P., Arnusch, C.J., Tour, J.M.: Laser-induced graphene by multiple lasing: toward electronics on cloth, paper, and food. ACS Nano **12**, 2176–2183 (2018)
46. Zhang, W., Lei, Y., Ming, F., Jiang, Q., Costa, P.M.F.J., Alshareef, H.N.: Lignin laser lithography: a direct-write method for fabricating 3D graphene electrodes for microsupercapacitors. Adv. Energy Mater. **8**, 1801840 (2018)
47. Quéré, D.: Wetting and roughness. Annu. Rev. Mater. Res. **38**, 71–99 (2008)
48. Nasser, J., Lin, J., Zhang, L., Sodano, H.A.: Laser induced graphene printing of spatially controlled super-hydrophobic/hydrophilic surfaces. Carbon **162**, 570–578 (2020)
49. Wu, W., Liang, R., Lu, L., Wang, W., Ran, X., Yue, D.: Preparation of superhydrophobic laser-induced graphene using Taro leaf structure as templates. Surf. Coat. Technol. **393**, 125744 (2020)
50. Li, Y., Luong, D.X., Zhang, J., Tarkunde, Y.R., Kittrell, C., Sargunaraj, F., Ji, Y., Arnusch, C.J., Tour, J.M.: Laser-induced graphene in controlled atmospheres: from superhydrophilic to superhydrophobic surfaces. Adv. Mater. **29**, 1700496 (2017)
51. Li, J.T., Stanford, M.G., Chen, W., Presutti, S.E., Tour, J.M.: Laminated laser-induced graphene composites. ACS Nano **14**, 7911–7919 (2020)
52. Luong, D.X., Yang, K., Yoon, J., Singh, S.P., Wang, T., Arnusch, C.J., Tour, J.M.: Laser-induced graphene composites as multifunctional surfaces. ACS Nano **13**, 2579–2586 (2019)
53. Parmeggiani, M., Zaccagnini, P., Stassi, S., Fontana, M., Bianco, S., Nicosia, C., Pirri, C.F., Lamberti, A.: PDMS/polyimide composite as elastomeric substrate for multifunctional laser-induced graphene electrodes. ACS Appl. Mater. Interfaces **11**, 33221–33230 (2019)
54. Ye, R., James, D.K., Tour, J.M.: Laser-induced graphene. Acc. Chem. Res. **51**, 1609–1620 (2018)
55. Tian, Q., Yan, W., Li, Y., Ho, D.: Bean pod-inspired ultra-sensitive and self-healing pressure sensor based on laser induced graphene and polystyrene microspheres sandwiched structure. ACS Appl. Mater. Interfaces **12**, 9710–9717 (2020)
56. Searle, A., Kirkup, L.: A direct comparison of wet, dry and insulating bioelectric recording electrodes. Physiol. Meas. **21**, 271–283 (2000)
57. Miyamoto, A., Lee, S., Cooray, N.F., Lee, S., Mori, M., Matsuhisa, N., Jin, H., Yoda, L., Yokota, T., Itoh, A., Sekino, M., Kawasaki, H., Ebihara, T., Amagai, M., Someya, T.: Inflammation-free, gas-permeable, lightweight, stretchable on-skin electronics with nanomeshes. Nat. Nanotechnol. **12**, 907–913 (2017)
58. Ferrari, L.M., Sudha, S., Tarantino, S., Esposti, R., Bolzoni, F., Cavallari, P., Cipriani, C., Mattoli, V., Greco, F.: Ultraconformable temporary tattoo electrodes for electrophysiology. Adv. Sci. **5**, 1700771 (2018)

59. Zucca, A., Cipriani, C., Sudha, Tarantino, S., Ricci, D., Mattoli, V., Greco, F.: Tattoo conductive polymer nanosheets for skin-contact applications. Adv. Healthc. Mater. **4**, 983–990 (2015)
60. Arduini, F., Micheli, L., Moscone, D., Palleschi, G., Piermarini, S., Ricci, F., Volpe, G.: Electrochemical biosensors based on nanomodified screen-printed electrodes: Recent applications in clinical analysis. TrAC Trends Anal. Chem. **79**, 114–126 (2016). Past, Present, Future Challenges of Biosensors and Bioanalytical Tools in Anal. Chem.: A Tribute to Prof Marco Mascini
61. Ge, L., Hong, Q., Li, H., Liu, C., Li, F.: Direct-laser-writing of metal sulfide-graphene nanocomposite photoelectrode toward sensitive photoelectrochemical sensing. Adv. Funct. Mater. **29**, 1904000 (2019)
62. Zhu, Z., Garcia-Gancedo, L., Flewitt, A.J., Xie, H., Moussy, F., Milne, W.I.: A critical review of glucose biosensors based on carbon nanomaterials: carbon nanotubes and graphene. Sensors **12**, 5996–6022 (2012)
63. Ge, L., Hong, Q., Li, H., Li, F.: A laser-induced TiO 2-decorated graphene photoelectrode for sensitive photoelectrochemical biosensing. Chem. Commun. **55**, 4945–4948 (2019)
64. Samouco, A., Marques, A.C., Pimentel, A., Martins, R., Fortunato, E.: Laser-induced electrodes towards low-cost flexible UV ZnO sensors. Flex. Print. Electron. **3**, 044002 (2018)
65. Mahmood, F., Zhang, C., Xie, Y., Stalla, D., Lin, J., Wan, C.: Transforming lignin into porous graphene via direct laser writing for solid-state supercapacitors. RSC Adv. **9**, 22713–22720 (2019)
66. Mahmood, F., Zhang, H., Lin, J., Wan, C.: Laser-induced graphene derived from Kraft lignin for flexible supercapacitors. ACS Omega **5**, 14611–14618 (2020)
67. Lei, Y., Alshareef, A.H., Zhao, W., Inal, S.: Laser-scribed graphene electrodes derived from lignin for biochemical sensing. ACS Appl. Nano Mater. **3**, 1166–1174 (2019)
68. Edberg, J., Brooke, R., Hosseinaei, O., Fall, A., Wijeratne, K., Sandberg, M.: Laser-induced graphitization of a forest-based ink for use in flexible and printed electronics. npj Flex. Electron. **4**, 1–10 (2020)
69. Peng, Z., Ye, R., Mann, J.A., Zakhidov, D., Li, Y., Smalley, P.R., Lin, J., Tour, J.M.: Flexible boron-doped laser-induced graphene microsupercapacitors. ACS Nano **9**, 5868–5875 (2015)
70. Li, L., Zhang, J., Peng, Z., Li, Y., Gao, C., Ji, Y., Ye, R., Kim, N.D., Zhong, Q., Yang, Y., Fei, H., Ruan, G., Tour, J.M.: High-performance pseudocapacitive microsupercapacitors from laser-induced graphene. Adv. Mater. **28**, 838–845 (2016)
71. Li, X., Cai, W., Teh, K.S., Qi, M., Zang, X., Ding, X., Cui, Y., Xie, Y., Wu, Y., Ma, H., Zhou, Z., Huang, Q.-A., Ye, J., Lin, L.: High-voltage flexible microsupercapacitors based on laser-induced graphene. ACS Appl. Mater. Interfaces **10**, 26357–26364 (2018)
72. d'Amora, M., Lamberti, A., Fontana, M., Giordani, S.: Toxicity assessment of laser-induced graphene by zebrafish during development. J. Phys.: Mater. **3**, 034008 (2020)
73. Cheng, H., Vepachedu, V.: Recent development of transient electronics. Theor. Appl. Mech. Lett. **6**, 21–31 (2016)
74. Wu, Y., Ye, D., Shan, Y., He, S., Su, Z., Liang, J., Zheng, J., Yang, Z., Yang, H., Xu, W., Jiang, H.: Edible and nutritive electronics: materials, fabrications, components, and applications. Adv. Mater. Technol. **5**, 2000100 (2020)